Princeton Plasma Physics Laboratory

PPPL-

PPPL-

Princeton Plasma Physics Laboratory
Report Disclaimers

PPPL Report Availability

Princeton Plasma Physics Laboratory:

http://www.pppl.gov/techreports.cfm

Office of Scientific and Technical Information (OSTI):

http://www.osti.gov/bridge

Related Links:

U.S. Department of Energy

Office of Scientific and Technical Information

Fusion Links

Generation of high non-inductive plasma current fraction H-mode discharges by high-harmonic fast wave heating in the National Spherical Torus Experiment

G. Taylor, J. C. Hosea, C. E. Kessel, B. P. LeBlanc, D. Mueller,

C. K. Phillips, E. J. Valeo, J. R. Wilson

Princeton Plasma Physics Laboratory, Princeton, New Jersey 08543, USA

P. M. Ryan

Oak Ridge National Laboratory, Oak Ridge, Tennessee 37831, USA

P. T. Bonoli, J.C. Wright

Plasma Science and Fusion Center, MIT, Massachusetts 02139, USA

R. W. Harvey

CompX, Del Mar, California 92014, USA

Abstract

1.4 MW of 30 MHz high-harmonic fast wave (HHFW) heating, with current drive antenna phasing, has generated a $I_p = 300kA$, $B_T(0) = 0.55T$ deuterium H-mode plasma in the National Spherical Torus Experiment that has a non-inductive plasma current fraction, $f_{NI} = 0.7 - 1$. Seventy-five percent of the non-inductive current was generated inside an internal transport barrier that formed at a normalized minor radius, $r/a \sim 0.4$. Three quarters of the non-inductive current was bootstrap current and the remaining non-inductive current was generated directly by HHFW power inside $r/a \sim 0.2$.

PACS# 52.55.Fa, 52.35.Hr

I. INTRODUCTION

The first experiments to generate high-confinement, or H-mode [1], plasmas in a tokamak using ion cyclotron range of frequency (ICRF) fast-wave heating alone were conducted in ASDEX in 1986 where ICRF power heated a deuterium plasma with a hydrogen minority [2]. Several years later H-mode plasmas were generated in DIII-D [3] by direct fast-wave heating of electrons, via Landau damping and transit time magnetic pumping [4, 5]. Fast-wave generated H-mode plasmas are now studied extensively in conventional larger aspect ratio tokamaks, such as Alcator C-mod [6], and ICRF fast-wave heating will heat the deuterium and tritium in ITER H-mode discharges [7, 8] to nuclear fusion temperatures. In this paper we present results for deuterium H-mode discharges generated and sustained by high-harmonic fast-wave (HHFW) heating in the National Spherical Torus Experiment (NSTX) [9], a low aspect ratio, spherical torus (ST) device. The ICRF heating in these experiments used current drive antenna phasing and was predominantly via direct fast-wave heating of electrons.

ST devices offer several advantages compared to conventional, larger aspect ratio, tokamaks, including a high ratio of plasma to confining magnetic field pressure, compact geometry, good confinement and relatively low confining magnetic field [10]. But because of the constraints imposed by the STs compact geometry it is critical to develop discharge initiation, plasma current (I_p) ramp-up, and plasma sustainment techniques that do not require a central solenoid. TSC [11] simulations of non-solenoidal plasma scenarios in NSTX [12] predict that HHFW heating [13] can play an important role in enabling the generation of an H-mode ST discharge with a high fraction of non-inductive plasma current, $f_{NI} \geq 1$.

The $f_{NI} \geq 1$ strategy developed for NSTX includes coupling 5-6 MW of HHFW power (P_{RF}) into a non-inductive, $I_p = 250 - 350 kA$, discharge that has been generated by coaxial helicity injection [14], outer poloidal field start-up [15] or plasma guns [16]. The HHFW heating will be used to drive I_p from ~ 300 kA to ~ 500 kA through the generation of an H-mode plasma with significant bootstrap current drive (BSCD) and direct RF current drive (RFCD). At I_p ~ 500 kA 90 keV deuterium neutral beam injection (NBI) in NSTX is sufficiently well confined to heat the plasma and generate additional BSCD and neutral beam injection current drive (NBICD).

The initial approach to developing this $f_{NI} \geq 1$ I_p ramp-up strategy on NSTX has been to heat a $I_p = 250 - 300kA$ flat top, inductively generated, deuterium plasma with HHFW power in order to drive the plasma into an H-mode with $f_{NI} \geq 1$. The first attempt at such an experiment was conducted on NSTX in 2005 [17]; the experiment used $P_{RF} \sim$ 2.7 MW to heat a $I_p = 250kA$, $B_T(0) = 0.45T$ plasma. These first experiments used an undirected antenna launch spectrum so that there was no directly generated RFCD, only BSCD. H-mode discharges with $f_{NI} = 0.65 - 0.8$ were produced but the H-mode phase, and the associated BSCD, could only be maintained for ~ 60 ms before the RF power tripped off. The RF power trips occurred because the plasma control system (PCS) latency was too large, so that the gap between the outer edge of the plasma and the HHFW antenna (outer gap) could not be maintained as the plasma stored energy suddenly increased at the L-mode (low-confinement) to H-mode transition (L-H transition). The resultant rapid change in outer gap after the L-H transition caused the reflected RF power to increase, resulting in the RF power being shut down. Following the shutdown of the RF power the plasma transitioned back to the L-mode and the RF power turned on again. This "L-H-L" cycle was repeated several times during each discharge.

Since 2005 there have been improvements in the PCS, discharge conditioning, and the HHFW antenna power feed design on NSTX that have allowed improved RF coupling to H-mode plasmas with no NBI. This paper reports results from an experiment run in 2010 that benefited from these improvements and that demonstrated a sustained $I_p = 300kA$, HHFW H-mode plasma that achieved $f_{NI} \sim 0.7 - 1$ with only $P_{RF} \sim 1.4$ MW and that used CD antenna phasing.

Since 2005 the PCS latency on NSTX has been significantly reduced and lithium conditioning has been introduced and found to increase the HHFW heating efficiency [18]. Also since 2005 higher magnetic field HHFW heating experiments have been conducted at $B_T(0) = 0.55T$ and these experiments exhibited better RF plasma coupling efficiency than experiments at $B_T(0) = 0.45T$ [19]. At the higher magnetic field the critical density for fast-wave propagation was moved further away from the front of the

HHFW antenna so that RF losses to the antenna and surrounding wall structures were reduced.

The NSTX HHFW antenna is located on the outboard midplane and extends 90° toroidally. It has 12 straps connected to six decoupled 30 MHz sources that can provide up to 6 MW of RF power to the antenna. The 30 MHz fast-waves launched by the antenna are resonant with the 7th-11th harmonics of the deuterium ion cyclotron resonance frequency when NSTX is operated at $B_T(0) = 0.55T$. The phase shift between adjacent antenna straps can be adjusted to launch a well-defined spectrum of directed waves to generate RFCD, with launched toroidal wavenumbers, $k_\phi = \pm 13 m^{-1}$, $k_\phi = \pm 8 m^{-1}$ and $k_\phi = \pm 3 m^{-1}$, when the phase difference ($\Delta\phi$) between adjacent antenna straps is ±150°, ±90° and ±30°, respectively [18-20]. Experiments reported here used $\Delta\phi$ =-90° and as a result generated co-I_p RFCD, in addition to BSCD. In contrast, the experiments run on NSTX in 2005 used $\Delta\phi$ =180°, an antenna phasing that launches a spectrum of waves with a combination of $k_\phi = \pm 14 m^{-1}$ and $k_\phi = \pm 18 m^{-1}$.

In addition to the above changes, modifications were made to the antennas between the 2005 and the 2010 HHFW experiments reported here. The single-feed, end-grounded HHFW antenna straps originally installed on NSTX were replaced in 2009 with double-feed, center-grounded straps to reduce the RF electric fields in the vicinity of the antenna Faraday shield for a given strap current. These RF electric fields were primarily responsible for the arcs that were limiting reliable high power operation to $P_{RF} \sim 3$ MW in 2008. After the double-feed upgrade late in the 2009 NSTX run campaign, reliable operation was obtained at $P_{RF} \sim 4$ MW after just a few days of antenna conditioning [21]. The results presented in this paper were obtained in 2010 with this new double-feed antenna configuration. Unfortunately in 2010 the maximum arc-free P_{RF} was limited to ≤ 1.4 MW due to a number of factors [22] that resulted in an increased accumulation of dust particles in the antenna environment. The arc-free power limit may also have been compromised during the 2010 run campaign, compared to earlier run campaigns, by the absence of boron conditioning at the beginning of the campaign and inter-shot glow discharge cleaning.

Section II presents experimental and modeling results and section III discusses the implications of these results and future plans for developing $f_{NI} \geq 1$ discharges in the NSTX upgrade (NSTX-U) [23] in 2014.

II. RESULTS

Most of the attempts to generate high f_{NI} HHFW $I_p = 300kA$ deuterium H-mode discharges in 2010 resulted in good initial RF heating and CD in the plasma core as the RF power ramped up, but core RF heating efficiency rapidly decayed soon after the L-H transition. Figure 1 summarizes the results from one of these discharges, shot 138498. The RF power was launched with a $k_\phi = -8m^{-1}$, co-I_p CD antenna phasing and was turned on at 0.16 s and ramped up to 1.4 MW in 100 ms, and then maintained at 1.4 MW from 0.26 s to 0.48 s (Fig. 1(b)). The outer gap was maintained at 0.08 to 0.1 m during the HHFW pulse until 0.35 s when it began oscillating between 0.05 and 0.15 m (Fig. 1(b)). If the outer gap is too large (> 0.1 m) there is poor coupling to the fast wave and if it is too small (< 0.05 m) the fast wave starts propagating near the antenna so that the RF power is deposited on the antenna and surrounding vacuum vessel structure. In this case the outer gap briefly falls below 0.05 m at 0.4 s, the reflected RF power increases, and the discharge drops out of H-mode. The line average density ($n_e L$) was 1.25x10^{19}m^{-2} at the start of HHFW heating, as measured by multi point Thomson scattering (MPTS) (Fig. 1(a), dashed line) and rises to about 2x10^{19}m^{-2} during the HHFW heating pulse. The central electron temperature ($T_e(0)$), measured by MPTS, (Fig. 1(a), solid line) increased from 0.2 keV at 0.16 s to 2 keV at 0.26 s as the HHFW power ramped to 1.4 MW and the plasma transitioned to H-mode. The plasma stored energy (W_{tot}) increased from 5 kJ at 0.16 s to 24 kJ at 0.3 s. After the H-mode transition $T_e(0)$ and W_{tot} decreased to 0.9 keV and 18 kJ, respectively, at 0.38 s. Figures 1(c) and 1(d) show the evolution of the n$_e$ profile ($n_e(R)$) and T_e profile ($T_e(R)$), respectively. At the start of HHFW heating (Fig. 1(c), 0.165 s, dashed line) $n_e(R)$ is peaked and $T_e(R)$ is flat (Fig. 1(d), 0.165 s, dashed line). At 0.282 s (thin solid line), after the H-mode transition the $n_e(R)$ profile has flattened, the density on axis remained at 1.5x10^{19} m^{-3} and a relatively steep edge pedestal developed. At 0.282 s $T_e(R)$ became very peaked with a central

value of 2 keV, consistent with good HHFW heating near the magnetic axis. At 0.382 s (thick solid line) $n_e(R)$ was still flat in the core with a central value of 2×10^{19} m^{-3}, but the edge pedestal was no longer as steep and $T_e(R)$ had broadened, indicative of poor HHFW heating near the axis.

The GENRAY ray tracing code [24] and the ADJ adjoint quasi-linear Fokker-Planck code [25] were used to model the RF heating and CD throughout the HHFW pulse on shot 138498. Figure 2 shows results at 0.282 s, near the time of peak $T_e(R)$ and W_{tot}. Figure 2(a) shows $T_e(r/a)$ (solid line) and $n_e(r/a)$ (dashed line) used for the modeling. 41 rays were launched at the last closed flux surface (LCFS) and these were followed until 99% of the RF power was absorbed. RF power losses in the scrape off were not included in the modeling, although these can be significant. Figure 2(b) plots the trajectory of the rays projected on the poloidal plasma cross-section. There was strong single pass RF power absorption, with the power being deposited near the midplane in the outer half of the plasma. A 3% hydrogen impurity was included but almost all the RF power was absorbed directly by electrons through Landau damping or transit-time magnetic pumping. Figure 2(c) shows profiles of the RF power deposition (solid line) and RFCD (dashed line) versus r/a at 0.282 s for 1 MW of RF power deposition inside the LCFS. Most of the RF power is deposited inside of $r/a \sim 0.5$, but RFCD is confined to the region inside $r/a \sim 0.3$ because of the extensive region of electron trapping on NSTX. The RFCD efficiency was 80 kA/MW. Later in time, at 0.382 s, RFCD efficiency calculated by GENRAY-ADJ dropped to 50 kA/MW, as a result of the higher n_e and lower T_e at that time. The HHFW coupling efficiency is defined as $\eta_{eff} \sim \Delta W_{tot}/(\tau * P_{RF})$, where ΔW_{tot} is the change in stored energy when HHFW power is coupled to the discharge and τ is the global energy confinement time. For shot 138498 $\eta_{eff} \sim 55\%$, so that at 0.282 s ~ 0.8 MW of RF power is absorbed inside the LCFS and generates about ~ 65 kA of RFCD.

The time evolution of the RF power deposition and RFCD for shot 138498 was also modeled with a version of the TORIC full-wave code [26] integrated into the TRANSP transport code [27]. This modeling also did not include RF coupling losses outside the LCFS; namely it assumed $\eta_{eff} = 100\%$. Figure 3 shows the time evolution of the RFCD

(dashed line) and the BSCD (thin solid line) for shot 138498. TRANSP-TORIC predicts 100 kA of RFCD at 0.282 s, similar to the 110 kA predicted by GENRAY-ADJ, and 140 kA of BSCD. Since $\eta_{eff} \sim 55\%$, the TRANSP-TORIC calculation implies 50 kA of RFCD, giving a total non-inductive current of 190 kA, or $f_{NI} \sim 0.65$ at 0.282 s.

In one discharge, shot 138506, $n_e L$ before the HHFW heating pulse was reduced to 0.75×10^{19} m^{-2}, about 40% lower than the other $I_p = 300kA$, $B_T(0) = 0.55T$ shots run during the experiment. As a result significantly better RF core heating was obtained during the H-mode phase for a period lasting $\sim$ 200 ms. Figure 4(a) shows the time evolution of $n_e L$, $T_e(0)$ and W_{tot} for shot 138506, and Fig. 4(b) shows the time evolution of P_{RF} and the outer gap. $n_e L$ remained lower than 138498 throughout the H-mode phase. $T_e(0)$ increased to 3 keV during the RF heating pulse, 50% higher than shot 138498, and unlike shot 138498, it kept rising until an antenna arc at 0.4 s shutdown the RF power for 20 ms. W_{tot} did not fall early in the H-mode phase, as it did during shot 138498. Notably the outer gap stayed between 0.05 and 0.1 m throughout the RF pulse and the discharge remained in the H-mode regime through the antenna arc at 0.4s. Figure 4(c) shows four density profiles measured by MPTS during shot 138506. $n_e(R)$ remained peaked until the L-H transition at 0.21s, at which time it developed a steep edge pedestal. At 0.29 s an internal transport barrier (ITB) formed at r/a $\sim$ 0.4 and then $n_e(R)$ became hollow inside the ITB. Unfortunately a motional Stark effect measurement of the current density profile was not available on the day of this experiment but it is possible that the RFCD near the core changed the local magnetic shear in the core enough to trigger the formation of the ITB. This behavior is similar to $f_{NI} \sim 1$ H-mode discharges that were generated with neutral beam injection in JT-60U when an ITB formed near a region of reversed magnetic shear [28].

Figure 5 shows GENRAY-ADJ results at 0.382 s, near the time of peak $T_e(0)$ and W_{tot} for shot 138506. $n_e(r/a)$ and $T_e(r/a)$ profiles used for the modeling at 0.382 s are plotted in Fig. 5(a). The 41 rays used in the calculation are plotted on the poloidal cross section in Fig. 5(b). Rays are plotted until 99% of the RF power is absorbed. As for shot 138498, there was strong single pass RF absorption of all the rays near the midplane in the outer half of the plasma and the RF power deposition profile was peaked on axis

(Fig. 5(c)). GENRAY-ADJ predicts 130 kA of co-I_p RFCD inside r/a ~ 0.2 for each MW of RF power deposited inside the LCFS. η_{eff} was estimated to be ~ 60% on shot 138506, yielding ~ 80 kA of RFCD.

The time evolution of the BSCD and RFCD during shot 138506, calculated by TRANSP-TORIC, is plotted in Fig. 6(a). Assuming $\eta_{eff} = 100\%$, there is 100-120 kA of RFCD is generated during the flat top of the RF heating pulse, (dashed line in Fig. 6(a)). The BSCD oscillates between 100 and 230 kA (thin solid line in Fig. 6(a)). These large BSCD fluctuations result from plasma pressure profile changes near the end of the RF power ramp-up (at 0.26 s), at the formation of the ITB (at 0.3 s) and inside the ITB (at 0.38 s) (Fig. 6(b)). Using $\eta_{eff} \sim 60\%$, $I_{RFCD} \sim 70$ kA at 0.382 s (Fig. 6(c)), slightly less than the value predicted by GENRAY-ADJ. Combining I_{RFCD} with the calculated $I_{BSCD} \sim 220$ kA gives $f_{NI} \sim 1$ at 0.382 s. Three quarters of the non-inductive current was generated inside the ITB. As a result of the large fluctuations in BSCD during the H-mode phase, f_{NI} varies between 0.7 and 1.

III. DISCUSSION

While the maximum arc-free HHFW P_{RF} was limited to ~ 1.4 MW in 2010 it was nevertheless possible to generate $I_p = 300kA$, $B_T(0) = 0.55T$ deuterium H-mode plasma with an $f_{NI} = 0.7-1$. This positive result was made possible by better outer gap control during he H-mode phase, so that the H-mode was sustained for ~ 250 ms, notably better than ~ 60 ms achieved in similar experiments on NSTX in 2005. Lower target densities made possible in part by using lithium conditioning, operation at higher $B_T(0)$, and CD antenna phasing significantly increased the f_{NI} achieved for a given P_{RF}. $f_{NI} = 0.7-1$ was obtained with about half the P_{RF} used in the 2005 NSTX experiments. However, there were still problems with maintaining an optimal outer gap for good HHFW coupling on many of the discharges. Even on the best discharge, shot 138506, there were large, rapid variations in BSCD due to changes in the core pressure profile. Clearly better control of the electron pressure profile is needed. In addition, motional Stark effect (MSE) measurements [29] of the current profile are important to benchmark the TRANSP-TORIC analysis and these were not available in 2010 on the day the

experimental results reported here were acquired. Experiments originally planned for 2011 to extend the generation of HHFW H-modes to higher arc-free P_{RF} in NSTX were cancelled when the NSTX experimental program was terminated due to a toroidal field coil failure. $f_{NI} \geq 1$ HHFW H-mode experiments with $P_{RF} \sim 4$ MW will resume in 2014 on NSTX-U, where it will be possible to run discharges with $B_T(0)$ up to 1 T. $f_{NI} > 1$, current overdrive experiments will attempt to ramp I_p from 300 to 500 kA with only HHFW power. Also a new MSE diagnostic that uses laser-induced fluorescence (MSE-LIF) [30] and that uses a low-power 30 keV diagnostic neutral beam, rather than requiring a more perturbing 90 keV high power NSTX heating beam will be available for current density profile measurements on NSTX-U.

ACKNOWLEDGEMENTS

REFERENCES

1. F. Wagner, G. Becker, K. Behringer, D. Campbell, A. Eberhagen, W. Engelhardt, G. Fussmann, O. Gehre, J. Gernhardt, G. V. Gierke, G. Haas, M. Huang, F. Karger, M. Keilhacker, O. Kluber, M. Kornherr, K. Lackner, G. Lisitano, G. G. Lister, H. M. Mayer, D. Meisel, E. R. Muller, H. Murmann, H. Niedermeyer, W. Poschenrieder, H. Rapp, H. Rohr, F. Schneider, G. Siller, E. Speth, A. Sta¨bler, K. H. Steuer, G. Venus, O. Vollmer, and Z. Yu, Phys. Rev. Lett. **49**, 1408 (1982).

2. K. Steinmetz, J.-M. Noterdaeme, F. Wagner, F. Wesner, J. Baumler, B. Becker, H. S. Bosch, M. Brambilla, F. Braun, H. Brocken, A. Eberhagen, R. Fritsch, G. Fussmann, O. Gehre, J. Gernhardt, G. v. Gierke, E. Glock, O. Gruber, G. Haas, J. Hofmann, F. Hofmeister, A. Izvozchikov, G. Janeschitz, F. Karger, M. Keilhacker, O. Kliiber, M. Kornherr, K. Lackner, G. Lisitano, E. van Mark, F. Mast, H. M. Mayer, K. McCormick, D. Meisel, V. Mertens, E. R. Muller, H. Murmann, H. Niedermeyer, W. Poschenrieder, S. Puri, H. Rapp, H. Rohr, F. Ryter, K.-H. Schmitter, F. Schneider, C. Setzensack, G. Siller,

P. Smeulders, F. Soldner, E. Speth, K.-H. Steuer, O. Vollmer, H. Wedler, and D. Zasche, Phys. Rev. Lett. **58**, 124 (1987).

3. N. J. Fisch and C. F. F. Karney, Phys. Fluids **24**, 27 (1982).

4. S. C. Chiu, V. S. Chan, R. W. Harvey, and M. Porkolab, Nucl. Fusion **29**, 2175 (1989).

5. C. C. Petty, R. I. Pinsker, M. J. Mayberry, M. Porkolab, F. W. Baity, P. T. Bonoli, S. C. Chiu, J. C. M. de Haas, R. H. Goulding, D. J. Hoffman, T. C. Luce, and R. Prater, Phys. Rev. Lett. **69**, 289 (1992).

6. E. S. Marmar and Alcator C-Mod Group, Fusion Sci. Technol. **51** 261 (2007).

7. D. W. Swain and R. H. Goulding, Fusion Eng. Des. **82**, 603 (2007).

8. E. F. Jaeger, L. A. Berry, E. F. D'Azevedo, R. F. Barrett, S. D. Ahern, D. W. Swain, D. B. Batchelor, R. W. Harvey, J. R. Myra[3], D. A. D'Ippolito, C. K. Phillips, E. Valeo, D. N. Smithe, P. T. Bonoli, J. C. Wright, and M. Choi, Phys. Plasmas **15**, 072513 (2008).

9. M. Ono, M. G. Bell, R. E. Bell, T. Bigelow, M. Bitter, W. Blanchard, D. S. Darrow, E. D. Fredrickson, D. A. Gates, L. R. Grisham, J. C. Hosea, D.W. Johnson, R. Kaita, S. M. Kaye, S. Kubota, H. W. Kugel, B. P. LeBlanc,R. Maingi, R. Maqueda, E. Mazzucato, J. Menard, D. Mueller, B. A.Nelson, C. Neumeyer, F. Paoletti, S. F. Paul, Y.-K. M. Peng, S.Ramakrishnan, R. Raman, P. M. Ryan, S. A. Sabbagh, C. H. Skinner, T.Stevenson, D. Stutman, D. W. Swain, E. J. Synakowski, G. Taylor, A.Von Halle, J. Wilgen, M. Williams, J. R. Wilson, S. J. Zweben, R. Ackers,R. E. Barry, A. Bers, J. M. Bialek, P. T. Bonoli, M. D. Carter, J. Chrzanowski, W. Davis, E. J. Doyle, L. Dudek, P. C. Efthimion, R. Ellis, J. R. Ferron, M. Finkenthal, E. Fredd, T. Gibney, R. J. Goldston, R. E. Hatcher, R. J. Hawryluk, H. Hayashiya, K. W. Hill, T. R. Jarboe, S. C. Jardin, H. Ji, M. Kalish, P. LaMarche, L. L. Lao, K. C. Lee, F. M. Levinton, N. C. Luhmann, R. Majeski, J. Manickam, R. Marsala, T. K. Mau, B. McCormack, S. S. Medley, M. M. Menon, O. Mitarai, M. Nagata, N. Nishino, G. Oliaro, H. K. Park, R. Parsells, G. Pearson, T. Peebles, C. K. Phillips, R. Pinsker, G. D. Porter, A. K. Ram, J. Robinson, P. Roney, A. L. Roquemore, A. Rosenberg, M. Schaffer, S. Shiraiwa, P. Sichta, D.Stotler, B. C. Stratton, Y. Takase, W. R. Wampler, G. A. Wurden, X. Q. Xu, J. G. Yang, L. Zeng, and W. Zhu, Nucl. Fusion **41**, 1435 (2001).

10. Y-K. M. Peng and D. J. Strickler, Nucl. Fusion **26**, 769 (1986).

11. S. C. Jardin, N. Pomphrey, and J. DeLucia, Comput. Phys. **66,** 481 (1983).

12. C.E. Kessel, E.J. Synakowski, M.E. Bell, D.A. Gates, R.W. Harvey[1], S.M. Kaye, T.K. Mau, J. Menard, C.K. Phillips, G. Taylor, R. Wilson and the NSTX Research Team, Nucl. Fusion **45**, 814 (2005).

13. P. M. Ryan, A. L. Rosenberg, D. W. Swain, J. R. Wilson, D. B. Batchelor, M. G. Bell, R. E. Bell, S. Bernabei, J. M. Bitter, P. T. Bonoli, M. Brambilla, A. Cardinali, M. D. Carter, D. Darrow, E. Frederickson, D. Gates, J. C. Hosea, E. F. Jaeger, S. M. Kaye, B. P. LeBlanc, R. Maingi, T. K. Mau, S. S. Medley, J. E. Menard, D. Mueller, M. Ono, F. Paoletti, Y-K. M. Peng, C. K. Phillips, R. I. Pinsker, D. A. Rasmussen, S. A. Sabbagh, E. J. Synakowski, J. B. Wilgen, and NSTX Team, in Proceedings of the 19th IAEA Fusion Energy Conference, Lyon, 2002, edited by M. Spak, IAEA, Vienna, 2003, Paper No. EX/P2-13.

14. R. Raman, D. Mueller, T.R. Jarboe, B.A. Nelson, M.G. Bell, M. Ono, T. Bigelow, R. Kaita, B. LeBlanc, K.C. Lee, R. Maqueda, J. Menard, S. Paul, and L. Roquemore, Nucl. Fusion **47**, 792 (2007).

15. W. Choe, J. Kim, and M. Ono, Nucl. Fusion **45**, 1463 (2005).

16. D. J. Battaglia, M. W. Bongard, R. J. Fonck, A. J. Redd, and A. C. Sontag, J. Fusion Energy **28**, 140 (2009).

17. C. E. Kessel, R. E. Bell, M. G. Bell, D. A. Gates, S. M. Kaye, B. P. LeBlanc, J. E. Menard, C. K. Phillips, E. J. Synakowski, G. Taylor, R. Wilson, and NSTX Research Team, Phys. Plasmas **13**, 056108 (2006).

18. G. Taylor, R. E. Bell, J. C. Hosea, B. P. LeBlanc, C. K. Phillips, M. Podesta, E. J. Valeo, J. R. Wilson, J-W. Ahn, G. Chen, D. L. Green, E. F. Jaeger, R. Maingi, P. M. Ryan, J. B. Wilgen, W. W. Heidbrink, D. Liu, P. T. Bonoli, T. Brecht, M. Choi, and R. W. Harvey, Phys. Plasmas **17**, 056114 (2010).

19. J. C. Hosea, R. E. Bell, B. P. LeBlanc, C. K. Phillips, G. Taylor, E. Valeo, J. R. Wilson, E. F. Jaeger, P. M. Ryan, J. Wilgen, H. Yuh, F. Levinton, S. Sabbagh, K. Tritz, J. Parker, P. T. Bonoli, R. Harvey, and NSTX Team , Phys. Plasmas **15**, 056104 (2008).

20. C. K. Phillips, R.E. Bell, L.A. Berry, P.T. Bonoli, R.W. Harvey, J.C. Hosea, E.F. Jaeger, B.P. LeBlanc, P.M. Ryan, G. Taylor, E.J. Valeo, J.B.Wilgen, J.R. Wilson, J.C. Wright, H. Yuh and the NSTX Team, Nucl. Fusion **49**, 075015 (2009).

21. P. M. Ryan, R. Ellis, J. C. Hosea, C. C. Kung, B. P. Leblanc, R. I. Pinsker, G. Taylor, J. R. Wilson, and the NSTX Team, "Operating The Upgraded NSTX HHFW Antenna Array In An Environment With Li-coated Surfaces", AIP Conf. Proc. **1406** (2011).

22. P. M. Ryan, A. McLean, J. C. Hosea, B. P. Leblanc, R. J. Perkins, G. Taylor, J. R. Wilson, R. I. Pinsker, and the NSTX Team, "Evaluation of the High Power Performance of the Upgraded NSTX HHFW Antenna", Bull. Am. Phys. Soc. **56**, 255 (2011).

23. J.E. Menard, J. Canik, B. Covele, S. Kaye, C. Kessel, M. Kotschentreuther, S. Mahajan, R. Maingi, C. Neumeyer, M. Ono, R. Raman, S. Sabbagh, V. Soukhanovskii, and P. Valanju, Proc. 37th European Physical Society Conf. on Plasma Physics (Dublin, Ireland, 2010), paper P2.106.

24. A. P. Smirnov and R.W. Harvey, Bull. Am. Phys. Soc. **40**, 1837 (1995).

25. A. P. Smirnov, R.W. Harvey, and R. Prater, Proc. 15th Workshop on ECE and ECRH, World Scientific (2009), pp. 301-306.

26. M. Brambilla, Plasma Phys. Control. Fusion **44**, 2423 (2002).

27. R. J. Hawryluk, in "Physics of Plasmas Close to Thermonuclear Conditions", Proc. of the International School of Plasma Physics, (Pergamon, Varenna, Italy, 1981) **1**, p. 19.

28. T. Fujita, S. Ide, Y. Kamada, T. Suzuki, T. Oikawa, S. Takeji, Y. Sakamoto, Y. Koide, A. Isayama, T. Hatae, H. Kubo, S. Higashijima, O. Naito, H. Shirai, and T. Fukuda, Phy. Rev. Lett. **87**, 085001 (2001).

H. Kubo, S. Higashijima, O. Naito, H. Shirai, and T. Fukuda

29. F. M. Levinton, R. J. Fonck, G. M. Gammel, R. Kaita, H. W. Kugel, E. T. Powell, and D. W. Roberts, Phys. Rev. Lett. **63**, 2060 (1989).

30. E. L. Foley and F. M. Levinton,. Rev. Sci. Instrum. **77**, 10F311 (2006).

FIGURE CAPTIONS

Figure 1

Time evolution of an I_p = 300kA HHFW-generated H-mode plasma (shot 138498) that did not maintain good HHFW coupling to the core during the H-mode phase. (a) Line integrated density ($n_e L$), central electron temperature ($T_e(0)$) and total plasma stored energy (W_{tot}) versus time. (b) Outer gap between the last closed flux surface and the front of the HHFW antenna on the midplane and RF power versus time. (c) Electron density and (d) electron temperature versus major radius at three times during shot 138498; 0.165 s, (dashed line), 0.282 s (thin solid line), and 0.382 s (thick solid line).

Figure 2

(a) $n_e(r/a)$ and $T_e(r/a)$ at 0.282 s, near the time of peaked $T_e(0)$ and W_{tot}, for shot 138498. (b) GENRAY-ADJ ray trajectories plotted on a poloidal cross section for shot 138498 at 0.282 s, each ray is followed until 99% of the power is absorbed. (c) GENRAY-ADJ RF power deposition (solid line) and RF-driven current (dashed line) versus r/a at 0.282 s for shot 138498.

Figure 3

I_p (thick solid black line), bootstrap current (I_{BSCD}, thin solid black line) and RF-driven current (I_{RFCD}, dashed line), calculated by TRANSP-TORIC, and P_{RF} (thick solid grey line) plotted as a function of time for shot 138498.

Figure 4

Time evolution of an I_p = 300kA HHFW-generated H-mode plasma (shot 138506) that maintained good HHFW coupling to the core during the H-mode phase. (a) Line integrated density ($n_e L$), central electron temperature ($T_e(0)$)) and total plasma stored energy (W_{tot}) versus time. (b) Outer gap between the last closed flux surface and the front of the HHFW antenna on the midplane and RF power versus time. (c) Electron density and (d) electron temperature versus major radius at four times during shot 138506; 0.165 s, (dashed line), 0.282 s (thin solid black line), 0.298 s (thick solid grey line) and 0.382 s (thick solid black line).

Figure 5

(a) $n_e(r/a)$ and $T_e(r/a)$ at 0.382 s, near the time of peaked $T_e(0)$ and W_{tot}, for shot 138506. (b) GENRAY-ADJ ray trajectories plotted on a poloidal cross section for shot 138506 at 0.382 s, each ray is followed until 99% of the power is absorbed. (c) GENRAY-ADJ RF power deposition (solid line) and RF-driven current (dashed line) versus r/a at 0.382 s for shot 138506.

Figure 6

(a) I_p (thick solid line), I_{BSCD} (thin solid line) and I_{RFCD} (dashed line) calculated by TRANSP-TORIC for shot 138506, and the RF power (Gray shading) plotted versus time. (b) Contour plot of the plasma pressure calculated by TRANSP-TORIC plotted versus r/a and time for shot 138506. Contours are plotted in kPa increments. (c) Area integrated current versus r/a calculated by TRANSP-TORIC at 0.382 s, including I_p (thick solid line), I_{BSCD} (thin solid line) and the I_{RFCD} (thin black line). The location of the internal transport barrier (ITB) is indicated by the shaded region near r/a = 0.4.
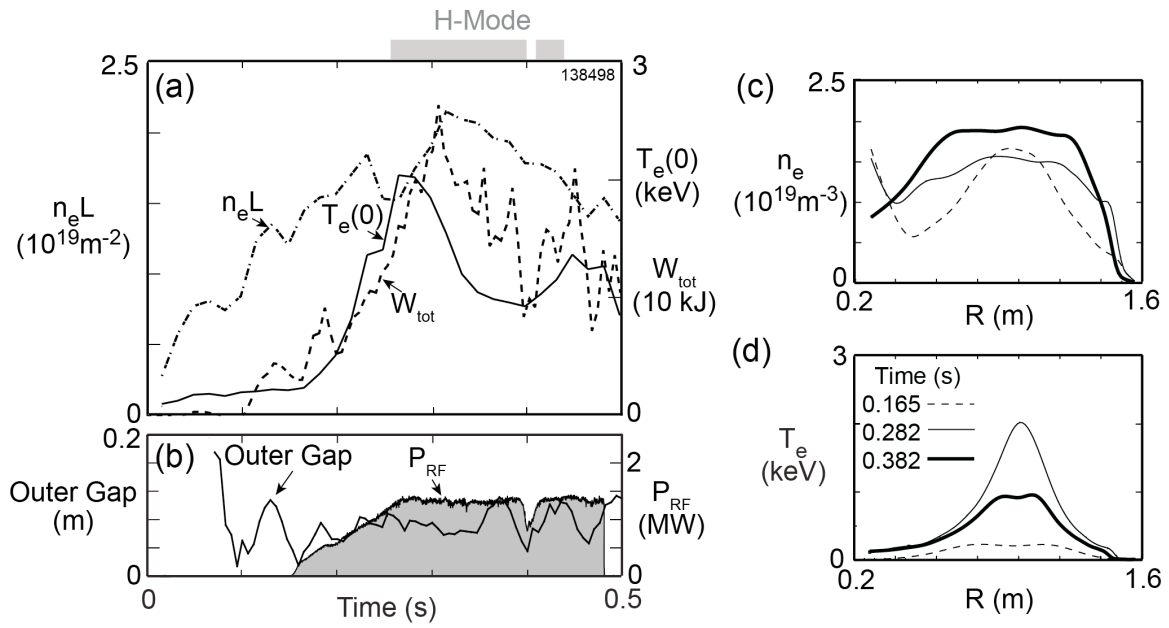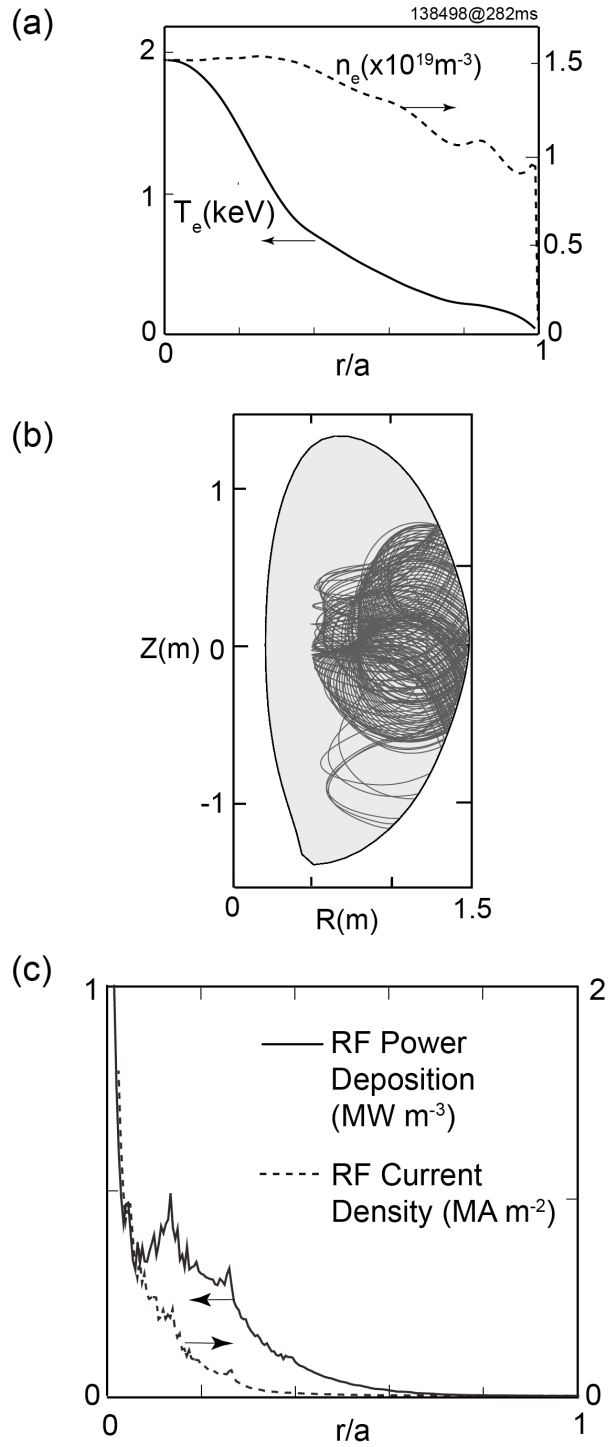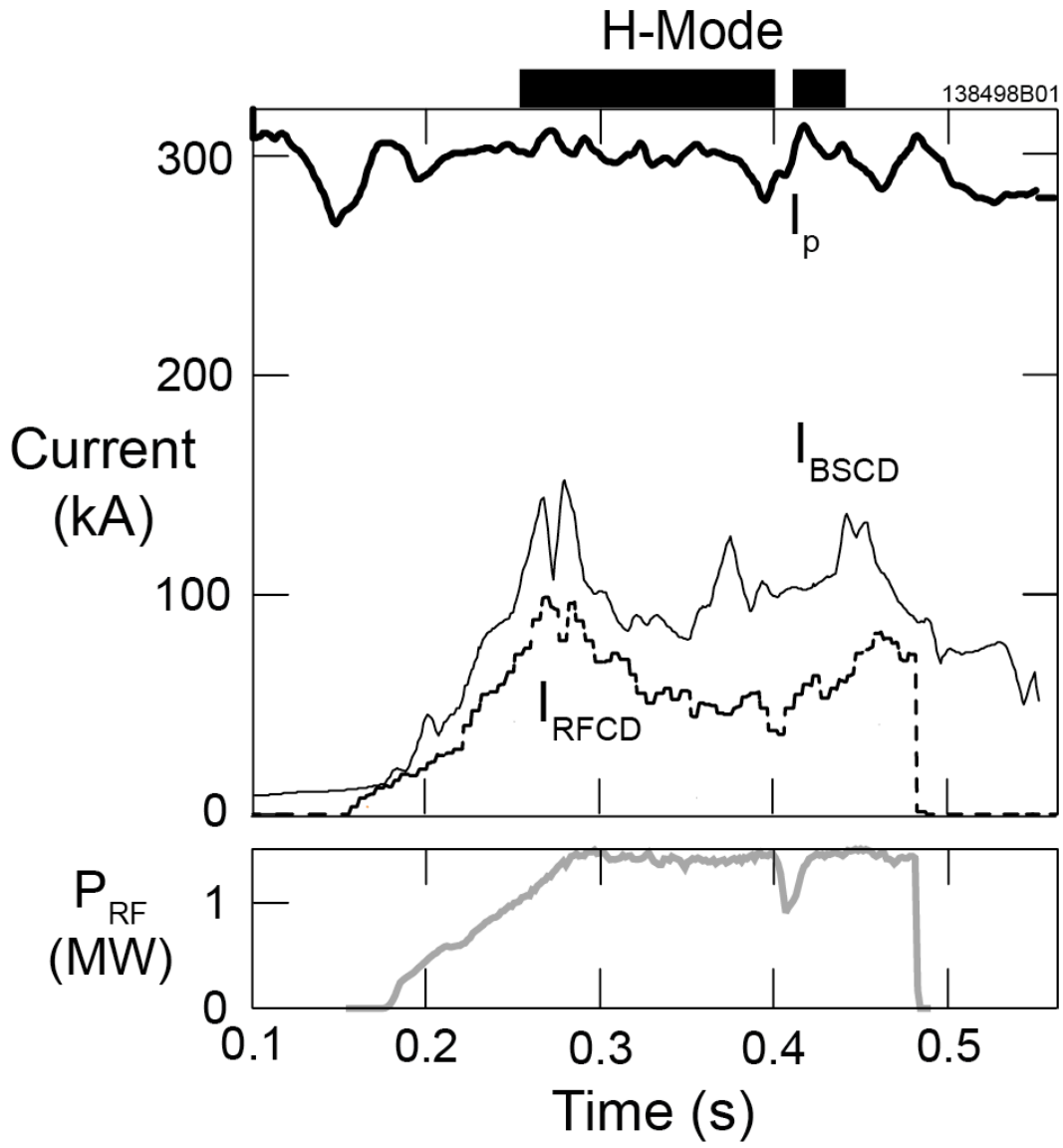
Figure 1

(a) 138498@282ms

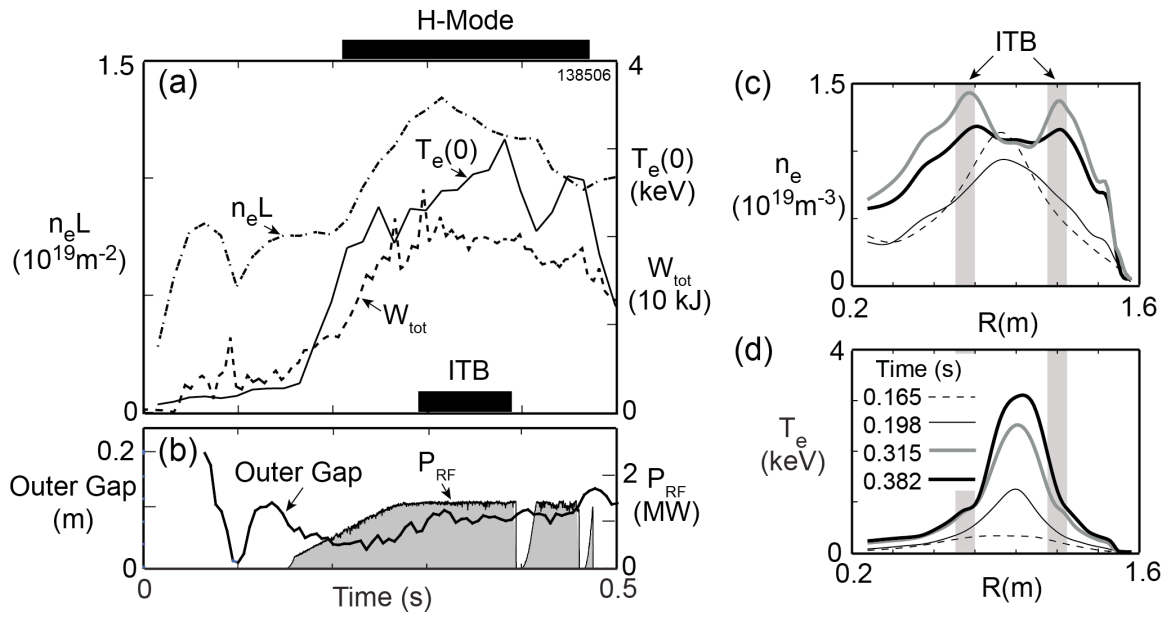(b)

(c)

Figure 2

16

Figure 3

Figure 4

(a)

138506@382ms

n_e (x10^{19}m^{-3})

T_e(keV)

r/a

(b)

Z(m)

R(m)

(c)

RF Power
Deposition
(MW m^{-3})

RF Current
Density (MA m^{-2})

r/a

Figure 5

19

(a) H-Mode

138506B03

Current (kA) — P_{RF} (MW)

I_p

I_{BSCD}

P_{RF}

I_{RFCD}

ITB

Time (s)

(b) Plasma Pressure Contours (kPa)

r/a

1
2
3
4
5
5

Time (s)

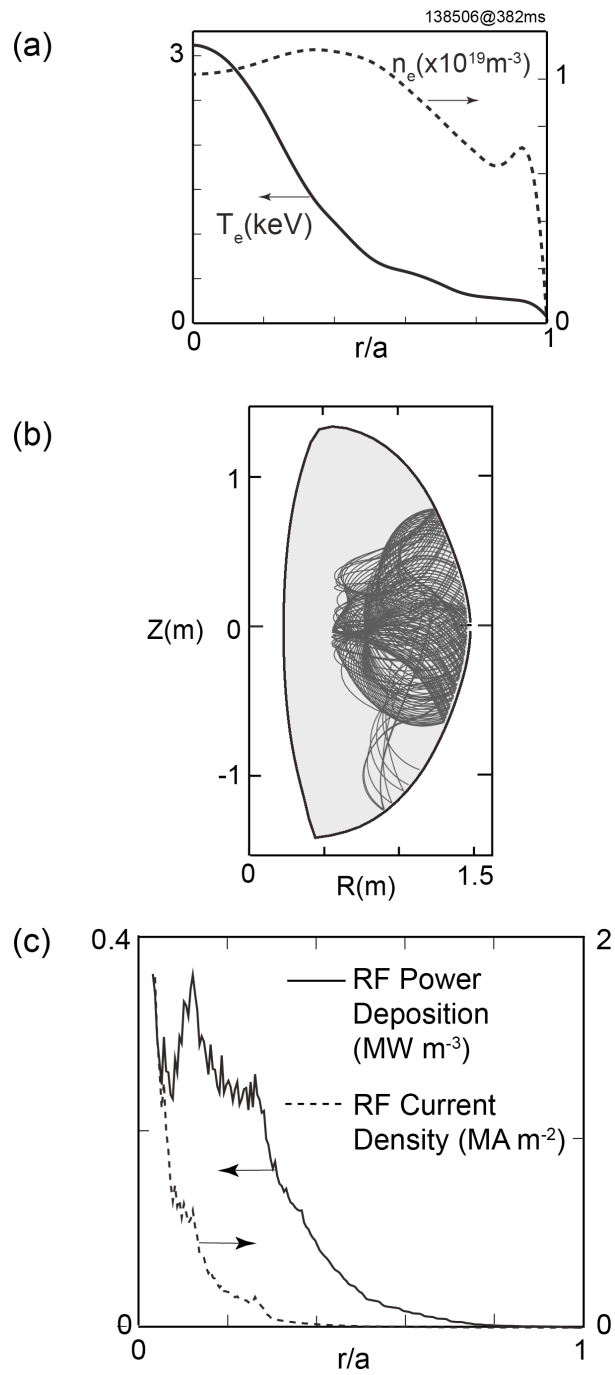(c) Area Integrated Current (kA)
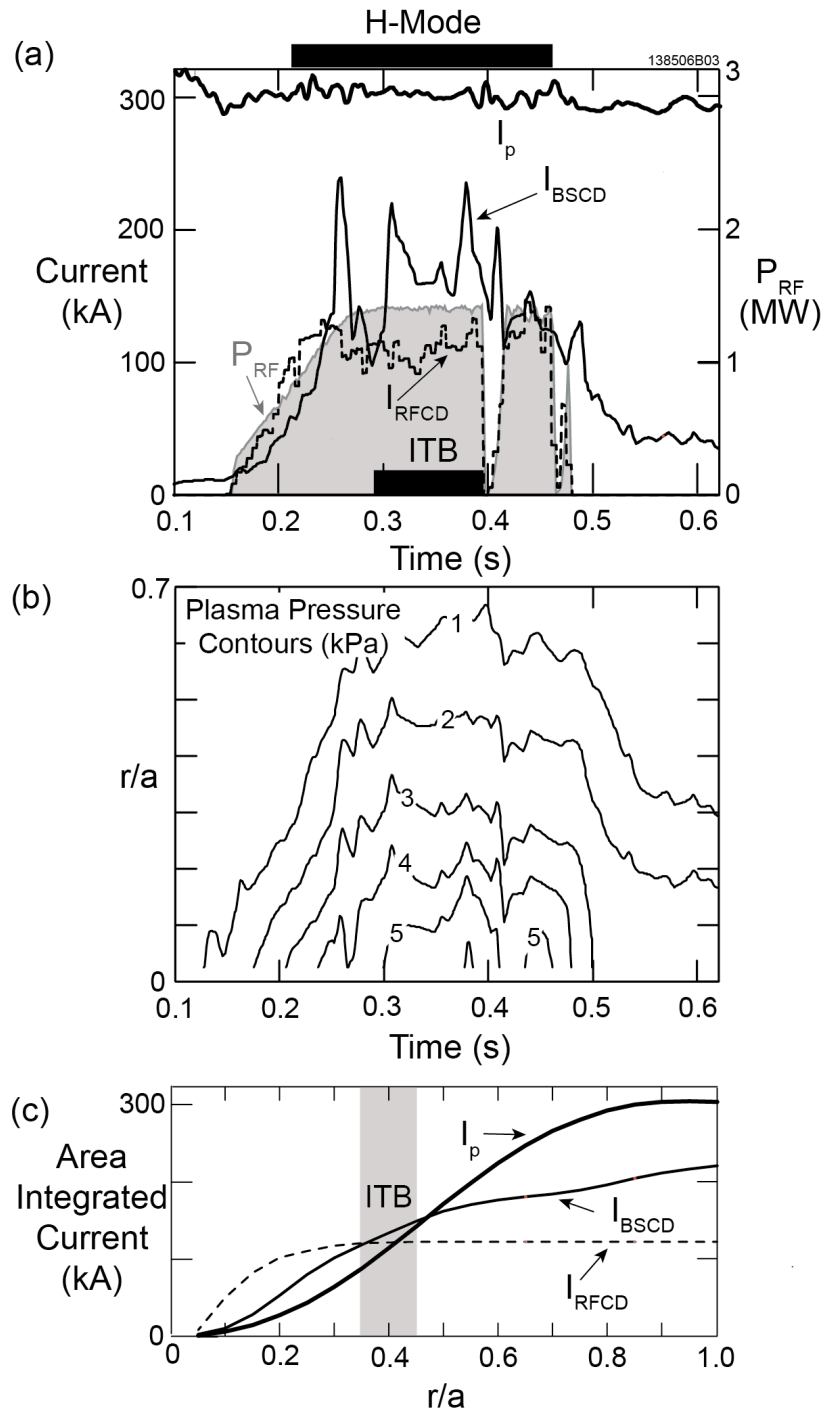
I_p

ITB

I_{BSCD}

I_{RFCD}

r/a

Figure 6

20

The Princeton Plasma Physics Laboratory is operated
by Princeton University under contract
with the U.S. Department of Energy.

Information Services
Princeton Plasma Physics Laboratory
P.O. Box 451
Princeton, NJ 08543

Phone: 609-243-2245
Fax: 609-243-2751
e-mail: pppl_info@pppl.gov
Internet Address: http://www.pppl.gov